Chapter 13
Impact of Support Settlement on the Seismic Fragility of a Substandard RC Frame with Plan Irregularity: Static Response and Fragility Assessment

Feras Abla, Shahin Huseynli, Ufuk Yazgan, and Onur Avci

Abstract Substandard reinforced-concrete (RC) buildings in seismic regions are susceptible to damage and collapse, particularly when differential foundation settlements coexist with earthquake excitation. This paper examines how support settlements alter (i) the gravity-load static response, and (ii) the seismic fragility of a three-story, plan-irregular, substandard RC frame (the SPEAR frame). A non-linear 3D OpenSees model is developed using fiber sections, plastic-hinge beam-column elements, and material constitutive laws calibrated to experimental data. Settlement scenarios (1, 2, and 3 cm) are imposed along axes X1, Y1, and simultaneously X1Y1. Gravity-only static analyses reveal pronounced axial-force and curvature/shear demand shifts in columns and beams near the settled axes and in the perpendicular framing direction. For 3 cm settlement, axial force in the critical interior column rises by up to 84% (two-axis case), and beam ends perpendicular to settlement reach or exceed yield curvature under gravity alone. Incremental Dynamic Analyses (IDA) and strain-based damage checks indicate that 1 cm settlement is sufficient to trigger slight damage even without seismic action; at 3 cm, the median collapse capacity drops by up to 9% depending on the settlement pattern. Findings underscore that settlement must be explicitly considered in performance assessments of substandard RC structures.

Keywords Differential settlement · Fragility analysis

Introduction

Substandard (RC frames in seismically active regions remain highly vulnerable to ground shaking. Past earthquakes, such as the 1999 Kocaeli and Düzce events in Turkiye, highlighted the poor performance of such structures, where noncompliance with seismic design codes led to widespread collapse [1]. These deficiencies are often tied to poor-quality materials, weak-column/strong-beam mechanisms, soft stories, and inadequate detailing, all of which significantly reduce seismic resilience. Differential support settlement compounds this vulnerability. Settlements can result from excavation activities, soil

Feras Abla(✉)
Graduate Student, Department of Civil and Environmental Engineering, Engineering Sciences Building, 1306 Evansdale Drive, West Virginia University, Morgantown, WV 26506
e-mail: fa00060@mix.wvu.edu

Shahin Huseynli
Postgraduate Researcher, School of Civil, Aerospace and Design Engineering, University of Bristol, Bristol, United Kingdom
e-mail: shahin.huseynli@bristol.ac.uk

Ufuk Yazgan
Professor, Disaster Management Institute, Istanbul Technical University, Istanbul, Turkey 34000
e-mail: ufukyazgan@itu.edu.tr

Onur Avci
Assistant Professor, Department of Civil and Environmental Engineering, Engineering Sciences Building, 1306 Evansdale Drive, West Virginia University, Morgantown, WV 26506
e-mail: onur.avci@mail.wvu.edu

© The Author(s), under exclusive license to River Publishers 2026

Kristin B. Zimmerman, PhD (eds.), *Dynamics of Civil Structures, 2026, Vol. 2*, Conference Proceedings of the Society for Experimental Mechanics Series, https://doi.org/10.13052/rp-9788743814139

liquefaction, or poor soil conditions, and when combined with seismic actions, they introduce additional flexural and shear demands that conventional assessment methods often overlook.

Several studies have investigated the impact of differential settlement on structural response. Early works [2, 3, 4] examined tolerance levels of buildings to settlement induced by their own weight, using deflection ratio and angular distortion as indicators. Later research expanded to excavation-induced settlements, showing that geometry and soil–structure interaction strongly influence stress redistribution in RC frames [5, 6, 7]. In seismic contexts, studies found that liquefaction-induced settlements significantly affect the vulnerability of substandard RC buildings [8, 9], with settlement-induced stresses accelerating progression toward damage states. More recently, [10, 11] demonstrated that settlement reduces collapse capacity in both RC and steel frames, with reductions of up to 15% reported for heavy damage states.

Against this backdrop, the present study examines the combined effect of settlement and seismic loading on the fragility of a substandard RC frame with plan irregularity. By focusing on static redistribution and seismic fragility analyses, it highlights how even modest support settlements can significantly alter internal force distributions, reduce displacement capacities, and increase collapse probabilities.

Case Study Building and Numerical Model

The SPEAR Frame

The case study is the full-scale, three-story SPEAR frame shown in Figure 1, which was pseudo-dynamic tested in full-scale at the European Laboratory for Structural Assessment (ELSA) at Ispra, Italy within the project of Seismic Performance Assessment and Rehabilitation of Existing Buildings (SPEAR). The frame is a gravity-designed, plan-irregular, and substandard RC building representative of poor seismic detailing building. Typical deficiencies include plain bars, sparse/poor stirrup detailing without 135° hooks, lap splices at column ends, strong-beam/weak-column proportions, and irregular plan geometry. Story height is 3.0 m (2.5 m clear), columns are predominantly 250×250 mm except one 250×750 mm wall-like column; beams are 250 mm web with 500 mm total depth including slab.

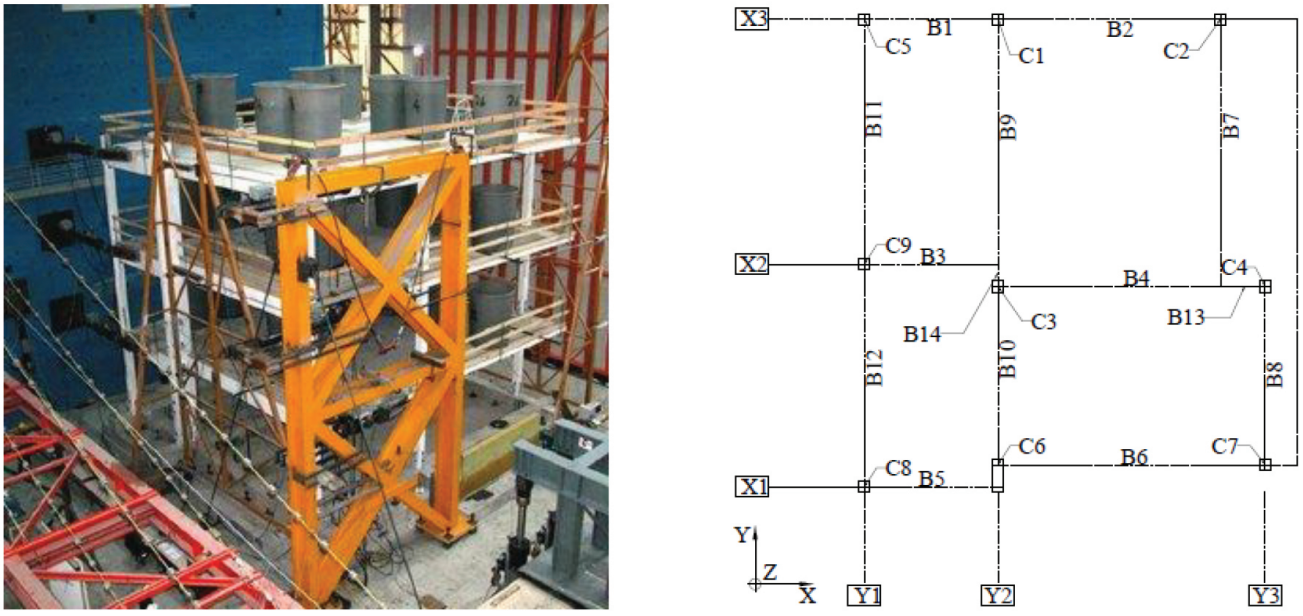

Fig. 1 SPEAR frame pseudo-dynamic test set up (a) (Courtesy [12]) and SPEAR frame layout (b).

Finite-Element Model

A three-dimensional OpenSees model (OpenSeesPy) [13] was developed to represent the substandard RC frame. Fiber sections were used to capture uniaxial material behavior, with beams modeled as T-sections according to an effective flange rule per span to account for slab participation. Torsional rigidity of the beams was increased to better reflect actual stiffness. Beam–column elements were modeled using beamWithHinges with Priestley-type plastic hinge lengths and Radau integration, except for element B14 where Gauss–Lobatto integration was adopted. P-Δ effects were incorporated, and rigid diaphragms were assigned at each floor level with the center of mass as the master node. Material behavior was simulated using Concrete04 for the confined core, Concrete02 for the unconfined cover, and the Giuffré–Menegotto–Pinto steel model with isotropic hardening for reinforcement [14]. To approximate bar slip and strain penetration effects observed in experiments, the steel initial tangent was reduced and hinge lengths were extended, reflecting premature cracking at joints. The applied loads included self-weight and tributary distributed loads, while lumped masses and mass moments of inertia were assigned to story centers of mass according to experimental data. Model validation demonstrated that the simulations successfully reproduced key experimental observations under bi-directional pseudo-dynamic testing, including peak third-story displacements (Figure 2) and story-drift envelopes, with acceptable bias in both principal directions.

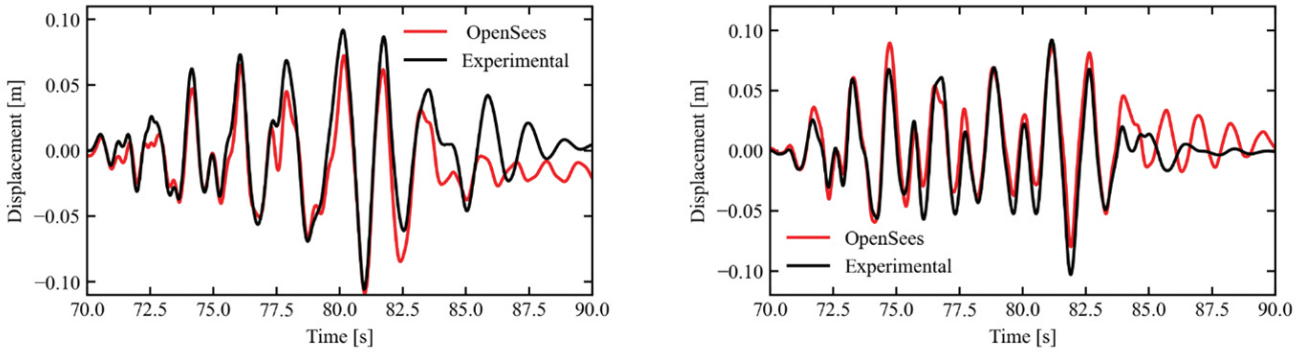

Fig. 2 The displacement time histories at the CM of the third story in both X (a) and Y (b) directions for PGA= 0.2g test.

Settlement Scenarios

Rigid-support vertical constraints are modified to impose settlements of 1, 2, and 3 cm along: (i) X1, (ii) Y1, and (iii) X1Y1 (two axes simultaneously). Gravity is applied in small increments to promote convergence with settlement-induced incompatibilities.

Analysis Method

Static Analysis under Gravity Loads

Gravity loads are applied with linear time series and small load steps using Newton iterations on a band-general solver with RCM numbering. Settlements are introduced via single-point constraints on base nodes of the targeted axes. Recorders capture axial forces in columns and curvature/shear demands at beam ends. Results are compared against the baseline (no settlement).

Fragility Assessment via IDA

IDA is conducted after gravity loads are established (held constant). Suites of ground motions are applied bi-directionally through uniform excitation with Newmark integration and Rayleigh damping. Damage states are defined using strain-based criteria consistent with low-ductility detailing (e.g., steel yield, concrete spalling at ε_c = 0.002, and ultimate concrete ε_c = 0.004 or shear failure for columns). For each settlement scenario, the fraction of records exceeding a limit state at intensity

measure (IM) levels is fit with a lognormal fragility (parameters by maximum likelihood), yielding median θ and dispersion β for slight (steel yielding), moderate (concrete spalling), and collapse (concrete crushing) damage thresholds.

Results: Static Redistribution under Settlement

Baseline (No Settlement)

Gravity-only demands concentrate axial force in the interior column (C3); soft-edge columns (X3/Y3) carry appreciable load. Beams show notable shear-capacity utilization in select spans even without settlement, but curvature demands remain well below ultimate capacities.

X1 Settlement

Figures 3a–3b illustrate the redistribution of internal forces in the beams under X1 settlements of 1–3 cm. The results highlight that settlement along this axis produces progressive increases in demand-to-capacity ratios for both yield curvature and shear forces, particularly in beams connected to or adjacent to the settled frame. The heatmap in Figure 3a shows that beams B8, B10, and B12 experience the sharpest rise in curvature demands. At 3 cm, the exceedance becomes critical, with B8 surpassing its yield curvature by over threefold, and B12 approaching similar levels. Shear demands (Figure 3b) also

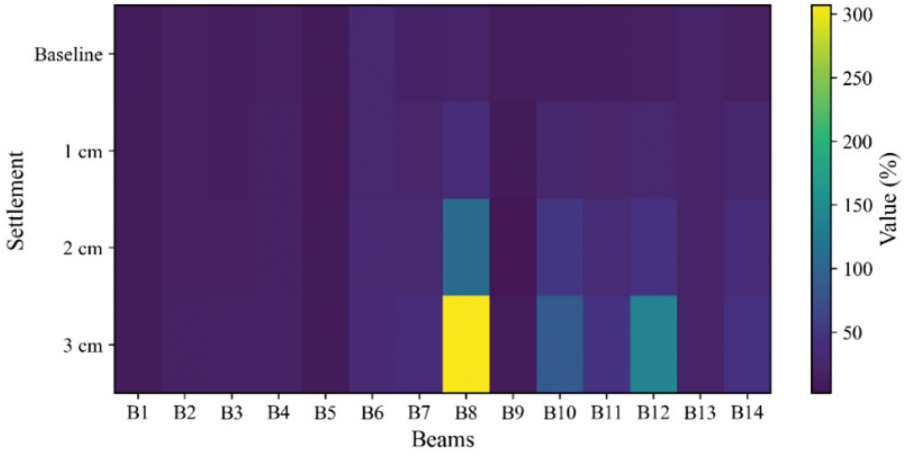

(a)

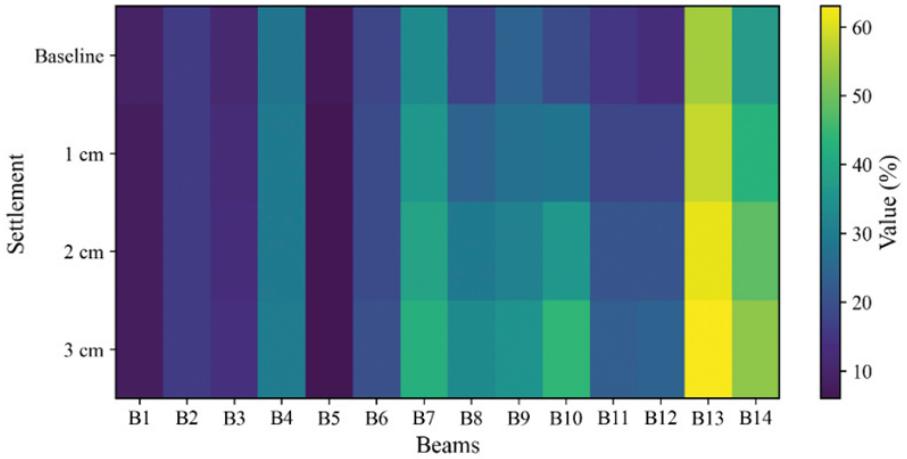

(b)

Fig. 3 Demand to capacity ratios for yield curvature (a), and shear force (b) for the X= 1–3 cm

escalate significantly; B13 and B14, already highly stressed in the baseline case, reach more than half of their shear capacity at 2 cm and continue to rise with increased settlement. Figure 4 further illustrates how the axial force ratios in columns redistribute, with C3 absorbing a much larger share of load, while columns in the settled frame (C6–C8) lose axial load, some dropping close to tension. This shift reduces ductility in C3 and C4 but enhances curvature capacity in the unloaded columns. Overall, the X1 settlement scenario demonstrates a clear concentration of demands on beams spanning between settled and adjacent frames, with a corresponding imbalance in axial load distribution across columns.

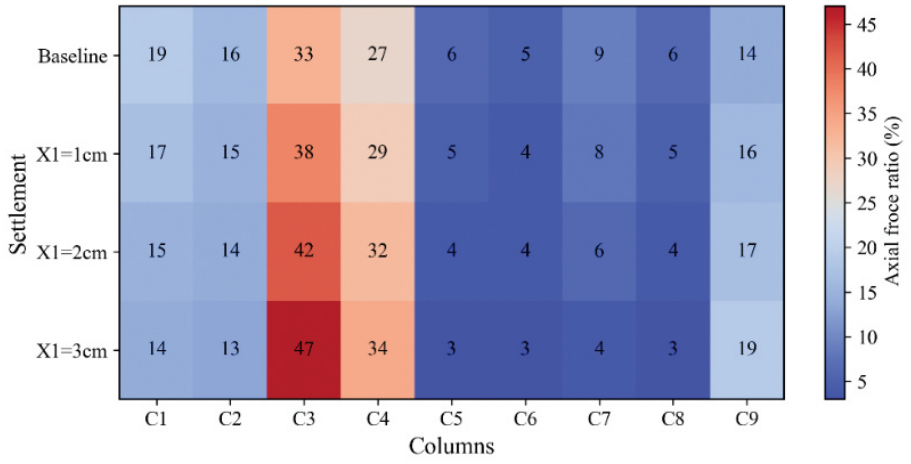

Fig. 4 Axial force ratio for X= 1–3 cm

Y1 Settlement

The redistribution pattern for the Y1 settlement scenario is presented in Figures 5a– 5b. Compared to the X1 case, settlements along Y1 exert more severe effects on beams aligned in the X-direction. As shown in Figure 5a, curvature demands on beams B1, B3, and B5 rise sharply, surpassing their yield capacities at 2 cm and 3 cm settlements. By 3 cm, B1 and B5 reach nearly four times their capacity. In terms of shear (Figure 5b), beams such as B4 and B14 approach critical demand levels, showing steep growth relative to the baseline. Column behavior is summarized in Figure 6, where the redistribution is evident: C1 and C3 accumulate higher axial loads, reducing their ultimate curvature capacities, while columns in the settled frame (C5 and C8) transition into tension. This redistribution reflects the asymmetry of the settlement influence, where beams orthogonal to the settlement axis suffer disproportionate increases in demand.

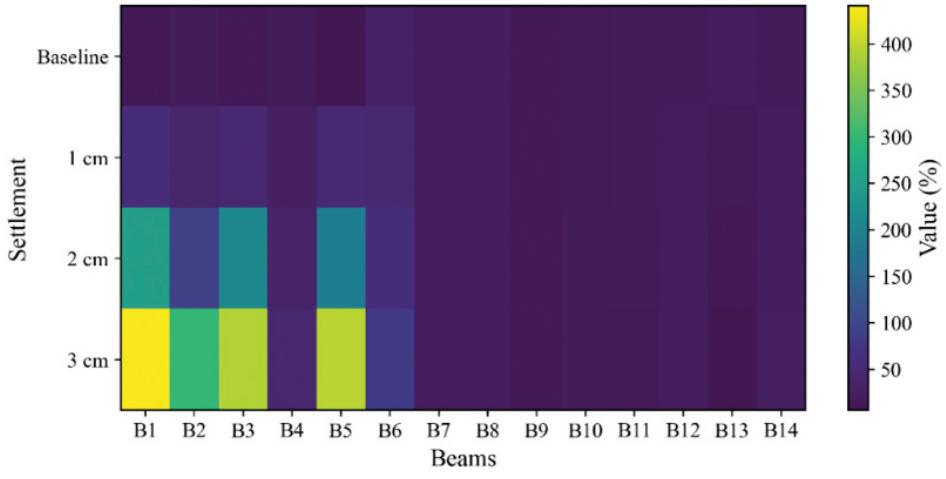

(a)

Fig. 5 *Continued*

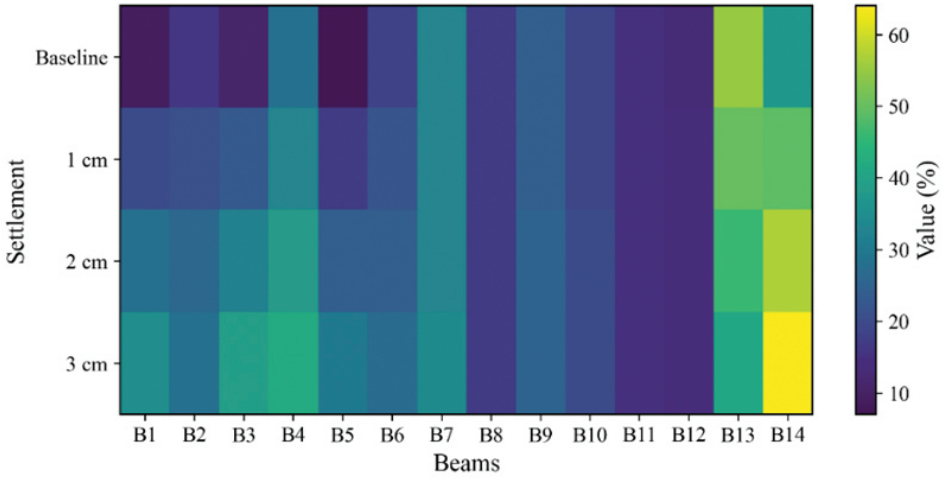

(b)

Fig. 5 Demand to capacity ratios for yield curvature (a), and shear force (b) for the Y= 1–3 cm

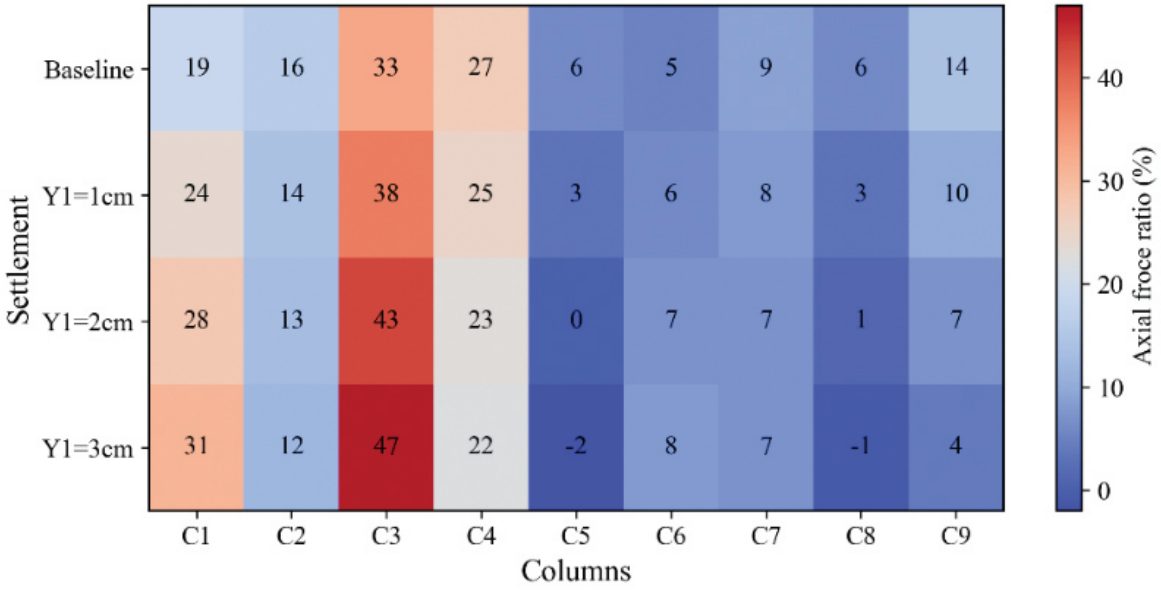

Fig. 6 Figure 4: Axial force ratio for Y= 1–3 cm.

X1Y1 Settlement (Two Axes)

Figures 7a– 7b display the combined settlement scenario where both X1 and Y1 frames undergo settlement simultaneously. This case produces the most severe redistributions, with both X- and Y-spanning beams heavily affected. Yield curvature demands (Figure 7a) are particularly critical in B1, B3, B8, and B10. At 3 cm settlement, B3 shows an eightfold exceedance of its yield capacity, while B8 and B10 also reach extreme levels. Shear demands (Figure 7b) rise steeply, especially in beams B1, B3, and B14, with B14 consuming up to 78% of its shear capacity. Figure 8 illustrates column axial redistribution: C3 becomes increasingly overloaded (approaching 60% axial force ratio at 3 cm), while several columns in the settled frames (C5, C6, C9) drop into near-zero or tensile loads. These shifts markedly reduce ductility in C3 while enhancing it in unloaded columns. The dual settlement case demonstrates how simultaneous differential settlements can push multiple members—both beams and columns—closer to critical states, magnifying the vulnerabilities observed in single-axis settlement scenarios

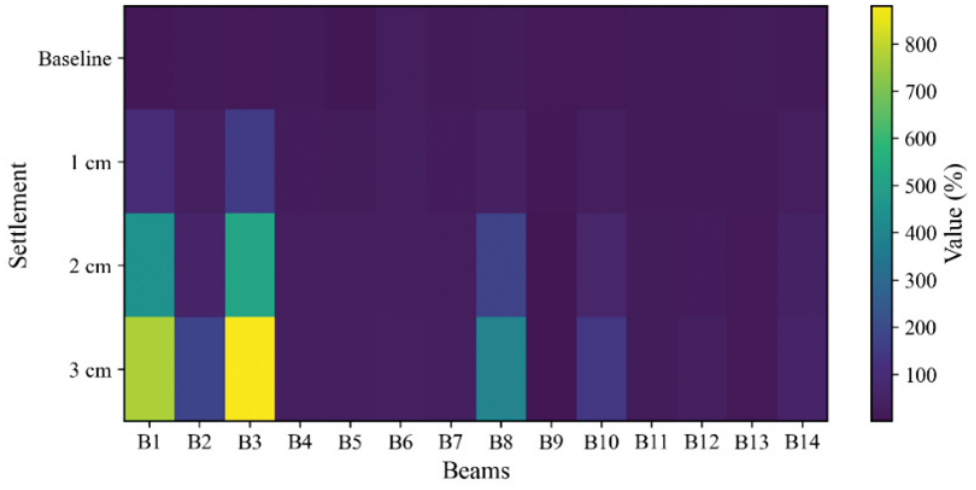

(a)

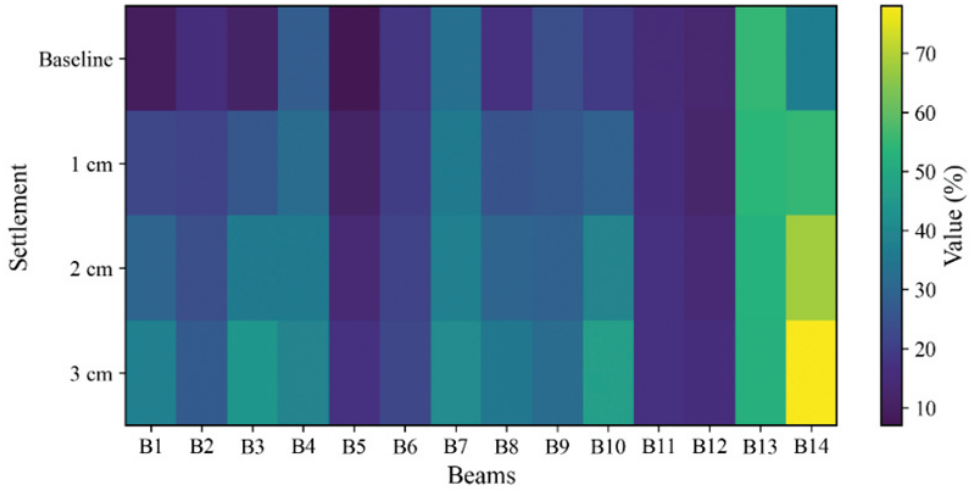

(b)

Fig. 7 Demand to capacity ratios for yield curvature (a), and shear force (b) for the XY= 1–3 cm

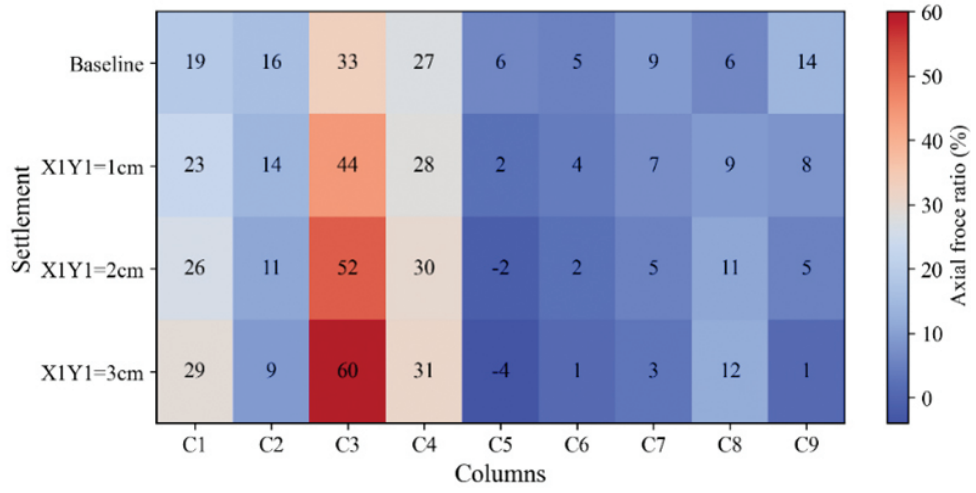

Fig. 8 Figure 6: Figure 4: Axial force ratio for XY= 1–3 cm.

Results: Seismic Fragility

Slight Damage State

Figure 9 illustrates the fragility curves for the slight damage state under all settlement scenarios. In the baseline case, the median capacity is already low (m = 3.8 cm/s), meaning the frame is vulnerable to even low levels of ground shaking. When differential settlement is introduced, the fragility curves in all cases confirm that as little as 1 cm of settlement is enough to induce slight damage without any seismic input. Increasing settlement magnitude (to 2 cm and 3 cm) does not affect the median significantly because the structural members have already reached their damage threshold at minimal excitation.

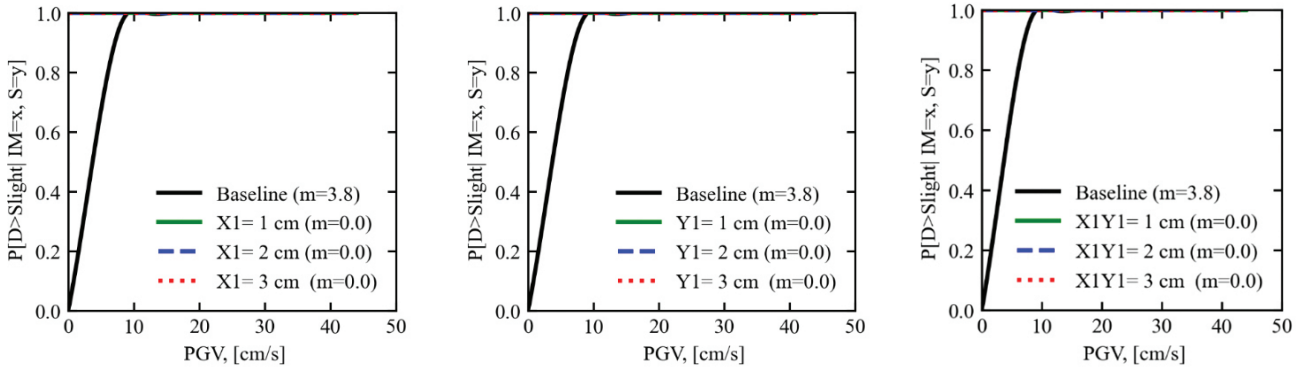

(a) (b) (c)

Fig. 9 Fragility curves for slight damage case

Moderate Damage State

For the moderate damage state (Figure 10), the baseline median PGV is about 9.9 cm/s. Settlement along X1 produces only minor reductions of 5–7% in the median capacity. In contrast, Y1 settlements of 1 cm and 2 cm slightly improve the median capacity by 10% and 7%, likely due to reductions in period and eccentricity favoring elastic response; however, at 3 cm, the capacity drops marginally by 1%. The X1Y1 case shows fluctuations between 10.9 cm/s and 9.8 cm/s, also reflecting the influence of reduced eccentricity ratios. Overall, the impact of settlement on the moderate damage state remains limited, with only small variations in capacity.

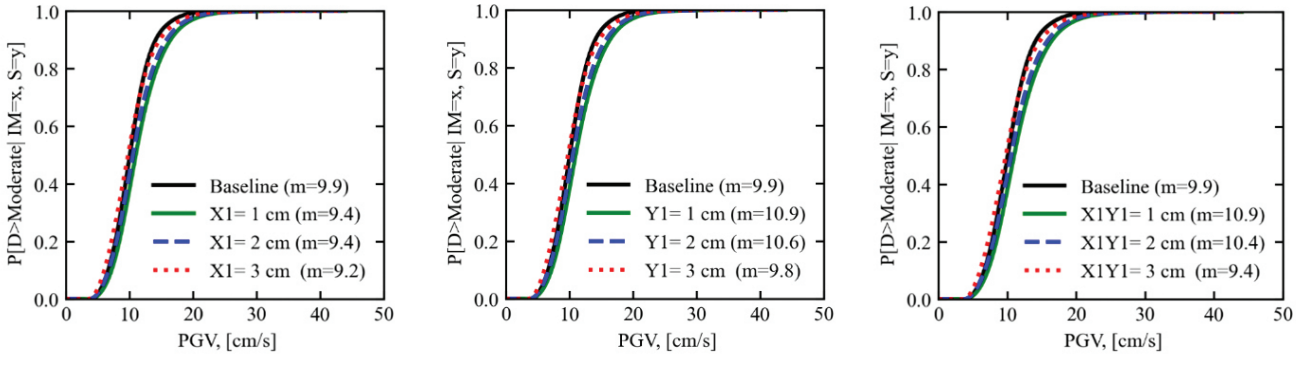

(a) (b) (c)

Fig. 10 Figure 9: Fragility curves for moderate damage case.

Ultimate Damage State

The most significant influence of settlement is seen at the ultimate damage state, as depicted in Figure 11. The baseline case shows a median capacity of approximately 22.1 cm/s PGV. Introducing settlement reduces this median progressively. For X1 (Figure 11a), the median decreases from 22.1 cm/s in the baseline to around 20.6 cm/s at 3 cm settlement. In the Y1 scenario (Figure 11b), the drop is even more marked, with the median reducing from 22.7 cm/s at 1 cm settlement to about 20.5 cm/s at 3 cm. The X1Y1 scenario (Figure 11c) demonstrates the steepest reduction, where the baseline median of 22.1 cm/s falls to about 20.3 cm/s under 3 cm settlement. This consistent trend confirms that settlement considerably reduces the collapse safety margin of the frame, lowering the ground motion intensity required to trigger ultimate damage. The combination of increased shear and curvature demands in beams and the redistribution of axial forces in columns explains the heightened fragility in this state. The results underscore that ignoring settlement in seismic assessments could significantly underestimate the likelihood of collapse for substandard RC frames

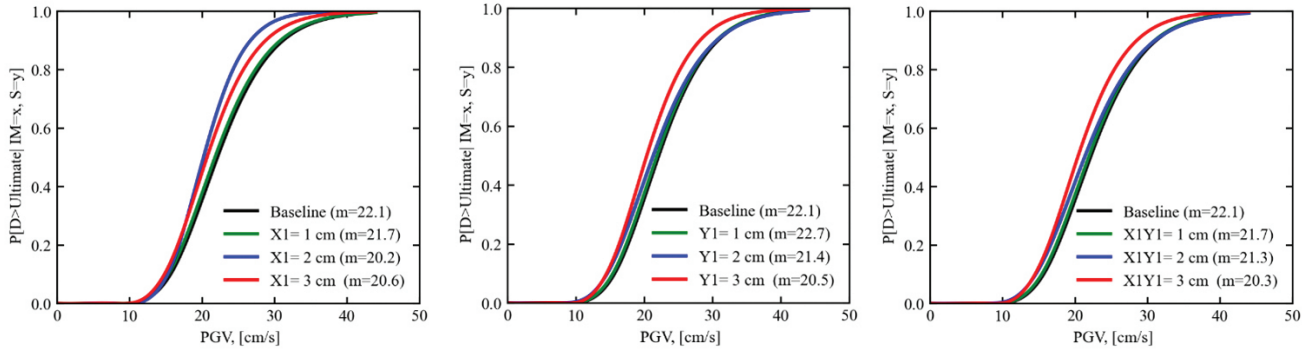

(a) (b) (c)

Fig. 11 Figure 10: Figure 9: Fragility curves for ultimate damage case.

Conclusions

The results demonstrate that support settlement significantly alters the behavior of substandard RC frames. Static analyses revealed that even small settlements cause major redistributions of internal forces. Beams spanning perpendicular to the settled axes experienced sharp increases in curvature and shear demands, in many cases exceeding yield capacities. Columns in the settled frames tended to unload, sometimes entering tension, while adjacent columns—especially C3—absorbed much higher axial forces, reducing their ductility. The combined X1Y1 settlement case produced the most severe effects, with widespread overstressing in both beams and columns and marked reductions in stiffness. Fragility analysis further confirmed that settlement amplifies seismic vulnerability. A differential settlement of only 1 cm was sufficient to place the frame in a slightly damaged state without seismic input. While moderate damage states showed limited sensitivity, ultimate damage states were highly affected. At 3 cm settlement, the median collapse capacity decreased by up to 9%, underscoring the reduction of the safety margin against failure.

These findings highlight the need to explicitly account for support settlement in the seismic assessment of existing substandard RC frames. Engineers should incorporate settlement effects into both static and dynamic analyses to avoid underestimating demands and collapse probabilities. Mitigation measures—such as soil improvement, foundation retrofitting, or redistribution of lateral resisting elements—should be prioritized in regions where poor soil conditions or excavation activities make differential settlement likely.

Acknowledgments The authors acknowledge the funding received from the Turkish Disaster and Emergency Management Presidency (AFAD) as a part of the project UDAP-Ç-21-34: “Monitoring of Surface Deformation in the Elazığ Sivrice Using Radar Remote Sensing.”.

References

1. Erdik, M. (2001). Report on 1999 Kocaeli and Düzce (Turkey) earthquakes. Structural control for civil and infrastructure engineering: World Scientific, 12, 149-186.
2. Skempton, A. W., & MacDonald, D. H. (1956). The allowable settlements of buildings. Proceedings of the Institution of Civil Engineers, 56, 727-768.
3. Meyerhof, G. G. (1953). Some recent foundation research and its application to design. The Structural Engineer, 316, 151-167.
4. Polshin, D. E., & Tokar, R. A. (1957, August). Maximum allowable non-uniform settlement of structures. In Proc., 4th Int. Conf. on Soil Mechanics and Foundation Engineering (Vol. 1, pp. 402-405). London: Butterworth's.
5. Boscardin, M. D., & Cording, E. J. (1989). Building response to excavation-induced settlement. Journal of Geotechnical Engineering, 1151, 1-21.
6. Laefer, D. F., Ceribasi, S., Long, J. H., & Cording, E. J. (2009). Predicting reinforced concrete frame response to excavation induced settlement. Journal of geotechnical and geoenvironmental engineering, 13511, 1605-1619.
7. Son, M., & Cording, E. J. (2011). Responses of buildings with different structural types to excavation-induced ground settlements. Journal of Geotechnical and Geoenvironmental Engineering, 1374, 323-333.
8. Fotopoulou, S., Karafagka, S., & Pitilakis, K. (2018). Vulnerability assessment of low-code reinforced concrete frame buildings subjected to liquefaction-induced differential displacements. Soil Dynamics and Earthquake Engineering, 110, 173-184.
9. Huseynli. S., Yazgan, U. (2021, October). Seismic Fragility Analysis of Seismically Deficient Buildings with Support Settlement. In Proceeding of 6th International Conference on Earthquake Engineering and Seismology.
10. Bao, C., Ma, X., Lim, K. S., Chen, G., Xu, F., Tan, F., & Abd Hamid, N. H. (2021). Seismic fragility analysis of steel moment-resisting frame structure with differential settlement. Soil Dynamics and Earthquake Engineering, 141, 106526.
11. Miano, A., Mele, A., & Prota, A. (2022). Fragility curves for different classes of existing RC buildings underground differential settlements. Engineering Structures, 257, 114077.
12. Jeong, S. H., & Elnashai, A. S. (2004). Analytical assessment of an irregular RD full scale 3D test structure.
13. McKenna, F., Scott, M. H., and Fenves, G. L. (2010) "Nonlinear finite-element analysis software architecture using object composition." Journal of Computing in Civil Engineering, 241:95-107.
14. Filippou, F. C., Popov, E. P., & Bertero, V. V. (1983). Effects of bond deterioration on hysteretic behavior of reinforced concrete joints.